Accepted Manuscript

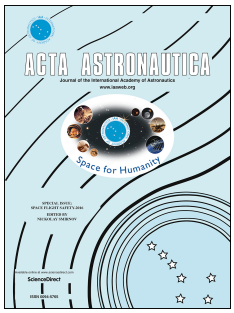

Numerical simulation of optical breakdown in a liquid droplet induced by a laser pulse

P.V. Bulat, O.P. Minin, K.N. Volkov

PII: S0094-5765(17)31545-X

DOI: 10.1016/j.actaastro.2017.11.029

Reference: AA 6560

To appear in: *Acta Astronautica*

Received Date: 30 October 2017

Revised Date: 16 November 2017

Accepted Date: 23 November 2017

Please cite this article as: P.V. Bulat, O.P. Minin, K.N. Volkov, Numerical simulation of optical breakdown in a liquid droplet induced by a laser pulse, *Acta Astronautica* (2017), doi: 10.1016/j.actaastro.2017.11.029.

Numerical Simulation of Optical Breakdown in a Liquid Droplet Induced by a Laser Pulse

P.V. Bulat[1, 2, *], O.P. Minin[3], K.N. Volkov[4]

[1]ITMO University, St Petersburg, Russia

[2]Baltic State Technical University, St Petersburg, Russia

[3]Public Joint-Stock Company "Tupolev", Moscow, Russia

[4]Kingston University, London, United Kingdom

Abstract

Modelling and simulation of interaction of laser pulse with individual liquid droplets are of crucial importance in terms of development and code coupling for simulation of laser propulsion and detonation in gas-droplet systems. These applications are challenging and complex for many reasons, one among them is the disparate time and length scales that are required to resolve for an accurate physical representation of the problem. The injection of liquid droplets with low evaporation temperature causes optical breakdown on the individual droplet and leads to a drop of the minimum pulse energy of detonation in the gas-droplet mixture. The mathematical models of various stages of the optical breakdown on individual droplet and numerical methodology for computer modelling of the laser-induced breakdown are developed. Sub-models of optical breakdown on liquid droplet include droplet heating to boiling temperature, its evaporation and formation of vapor aureole around the droplet, ionization of vapor aureole and development of electron avalanche, appearance of micro-plasma spots and their expansion, propagation of shock wave inside the droplet and in the surrounding gas. The threshold intensity of optical breakdown on individual water droplet and its dependence on droplet radius, location of droplet, total energy and radius of laser pulse are studied.

Keywords

Flight safety; Laser propulsion; Laser pulse; Droplet; Numerical simulation; Optical breakdown; Threshold intensity; Shock wave

1 Introduction

Interaction of a laser pulse with gas-droplet mixtures plays an important role in the design and improvement of propulsive characteristics of pulse detonation engines [1–4]. Laser propulsion using water droplets as a propellant is considered to have a wide range of future aerospace applications [5]. There are similarities between the laser-induced acoustic shock waves and those associated with blast waves and sonic booms. The acoustic pulses associated with laser-induced sparks could be used in the laboratory to simulate blast sounds from explosions or sonic booms and to investigate the associated propagation effects [6]. The propagation of laser beams in the atmosphere involves the interaction of high power or high

*Corresponding author: pavelbulat@mail.ru

peak intensity pulses with atmospheric aerosols which can alter the beam energy delivery and its spatial characteristics over long propagation lengths [7].

In order to have a more efficient propulsive effect with a minimum consumption of water and for safe transportation of laser radiation through gas-droplet flows, further studies on interaction of laser pulse with individual droplets have become more important.

When a high-power laser pulse ($I \sim 10^{11}$ W/cm^2) is focused at a point and interacts with a gas, the gas is heated to temperatures of thousands of degrees within several microseconds, breaking down and becoming highly ionized. This process, laser-induced breakdown (LIB), is always accompanied by a light flash and generation of sound (acoustic shock wave). Droplets, trapped by a laser beam, considerably influence results of the LIB. There is a threshold intensity of the laser pulse at which intense evaporation of the droplet leads to heat destruction of the droplet either by means of local jetting of the essential part of the droplet mass or due to an explosion of the droplet (optical breakdown).

During optical breakdown, a high free electron density (a plasma) of the order of 10^{18}–10^{20} electrons/cm^3 is produced [8]. Two mechanisms are responsible for gas ionization [9]: multi-photon ionization and cascade ionization (it is also referred as electron avalanche or impact ionization). Multi-photon absorption results when a molecule simultaneously absorbs enough photons to ionize the molecule and occurs when the incoming laser irradiance exceeds a threshold intensity. Avalanche ionization (electron cascade) is initiated when free electrons present in the material absorbing the laser energy. Seed electrons absorb laser energy by favorable collisions with heavier particles (molecules and ions). If the electrons sustain enough favorable collisions, they gain sufficient energy to impact ionize other molecules, freeing new electrons to repeat the process, which results in a geometric increase in the free electron density. For long pulses (in the microsecond regime), LIB is primarily caused by avalanche ionization, while multi-photon absorption dominates breakdown in the low femtosecond regime [10]. Both multi-photon absorption and avalanche ionization depend on the laser intensity and require a minimum threshold intensity before breakdown is initiated [11].

Many experimental and computational studies have been performed on the interaction between single droplets and focused laser beams demonstrating the influence of droplet size and other parameters on the breakdown process. A physical model describing the process of the laser and water droplet interaction is proposed in [12, 13]. It has been shown that the droplet acts like a lens and focuses the laser light with ignition occurring on the shadow side of the droplet in either the gas or liquid phase. Once breakdown has occurred, plasma is vented from the droplet away from the laser and explosive vaporization of the droplet occurs. The breakdown energy is a function of droplet and gas material, droplet size, and this is over two–three orders of magnitude smaller than for pure gas ignition [14].

Experiments on the LIB of large transparent liquid droplets are reviewed in [15]. LIB is linked with non-linear optical effects in droplets. A micrometer-sized transparent droplet acts as an optical cavity to provide feedback for the internally generated non-linear radiation. The schematic pattern of the LIB is supported with the experiments [16]. When a water droplet is irradiated by a high power laser pulse, the laser-induced plasma reaches a maximum speed of 20 km/s. Experimental study on the vaporization of fog droplets subjected to CO_2 laser irradiation is performed in [17, 18].

A water droplet is nearly transparent for laser radiation. The Lorenz–Mie calculations give a result such that the droplet concentrates the input intensity I_0 at three locations around the principal diameter [19]: outside the droplet near the shadow face with intensity about $\sim 10^3 I_0$, inside the droplet near the shadow face with intensity larger than $10^2 I_0$, inside the droplet near the illuminated face with intensity about $10^2 I_0$. These enhanced

intensities lower the threshold intensity in the droplet and in the surrounding gas. Optical effects in micro-sized droplets are reviewed in [20]. Mie scattering and related computational methods are discussed in [21].

When the droplet is hit by a laser pulse with high energy a part of the liquid is converted into a plasma state. This laser-induced phase change is the driving force of the fluid dynamics. The complete vaporization or explosion of micrometer-sized droplets results from the linear absorption of laser energy [22]. Self-focusing and dielectric breakdown leads to plasma formation in transparent droplets [23]. Laser impact has also been used to generate liquid motion by vaporization or plasma formation in confined geometries [24, 25].

The explosive evaporation of water droplets is discussed in [26–29]. For water droplets of radius from 50 to 200 μm, the process of explosive evaporation occurs at a temperature 10^3 K. Shock waves arising as a result of expansion of a droplet and high pressure within the droplet are treated as the mechanism triggering an optical breakdown [26]. The explosive evaporation of the droplet is attributed to the emergence and growth of vapor bubbles within the droplet [27,28], when the liquid temperature reaches that of explosive boiling (for water, this temperature at normal pressure is 578 K). It is suggested that if there are impurities in the water droplets, the breakdown could be initiated inside the droplet first and later on in the air surrounding the droplet [29].

The heating of the plasma depends dramatically on the laser parameters (duration, pulse shape, and intensity) on one hand, and on the droplet diameter on the other [30].

The explosive vaporization of a single droplet by high-power laser radiation is investigated in [31]. The optical size of the droplet is assumed to be in the Rayleigh limit (it absorbs energy uniformly). Uniform absorption leads to the spherically symmetric motion, and a one-dimensional simulation is sufficient to describe the flow. The duration of the pulse is so short that no fluid motion occurs during the pulse. The slow vaporization regime considered incorporates molecular transport effects but assumes a constant pressure field, thus eliminating convection. Breakdown is not considered, but the results obtained support the possibility of ionization in the shock-heated air.

A model for simulating the LIB in air and behind droplets is developed in [11]. A direct Monte Carlo simulation is presented taking into account energy losses via ionization, vibrational and excitational losses. The light field distribution behind spherical droplet is described by Mie theory which gives an analytical solution of the Maxwell equations for spherical boundary conditions. Computational as well as experimental results are presented varying the gas pressure, laser pulse length, focal spot size and droplet size. The breakdown in the presence of droplets shows a much steeper dependency on increasing gas pressure and droplet size than breakdown in air without droplets. The combined effect of increasing Mie intensities behind larger droplets and the increasing focal spot size results in a significant decrease of the threshold intensity by almost two orders of magnitude for larger droplets.

Processes that control transport and optical breakdown on droplets remain unresolved and introduce significant uncertainties into modelling and simulation [32]. The most important parameter for practical applications is the threshold intensity of laser pulse required for optical breakdown on individual droplet. Physical and mathematical models of LIB on individual droplet and numerical methodology for computer modelling of laser-induced breakdown are developed in this study. Mathematical models of various stages of the optical breakdown are derived and applied to the analysis of LIB on micrometer-sized water droplets. The threshold intensity of optical breakdown and its dependence on input parameters such as droplet radius, location of droplet, total energy of laser pulse and radius of laser spot, are studied. Comparison of some numerical results with experimental data is made.

2 Breakdown mechanism

The explosive vaporization of a single droplet by pulsed laser radiation is considered. In the explosive vaporization regime, molecular transport effects such as mass diffusion and heat conduction are small compared to convective transport. Convective transport is driven by gradients in the pressure field. Convection becomes important when the vapour pressure of the evaporating droplet becomes comparable to the pressure of the surrounding gas. The lowering of the breakdown potential has been attributed to shock heating of the atmosphere.

The high-intensity laser beam interacts with a single droplet those radius is much larger than the laser wavelength. The rate at which the heat is generated determines the response of the droplet. The heating rate varies over a wide range, as determined by the complex index of refraction, the intensity of the radiation source and the optical size of the droplet. The optical size (Mie size parameter) is defined as $x = 2\pi r_s/\lambda$, where r_s is the droplet radius and λ is the wavelength of the incident light.

As the input laser intensity, I_0, increases from low to medium, and to high values, the LIB processes is shown schematically in the Figure 1, where τ is time of laser pulse. The specific example is for a liquid droplet with a high LIB threshold I_B in a gas and with a low LIB threshold I_A in the droplet [19]. The schematic pattern of the LIB is supported with the experiments reported in [16].

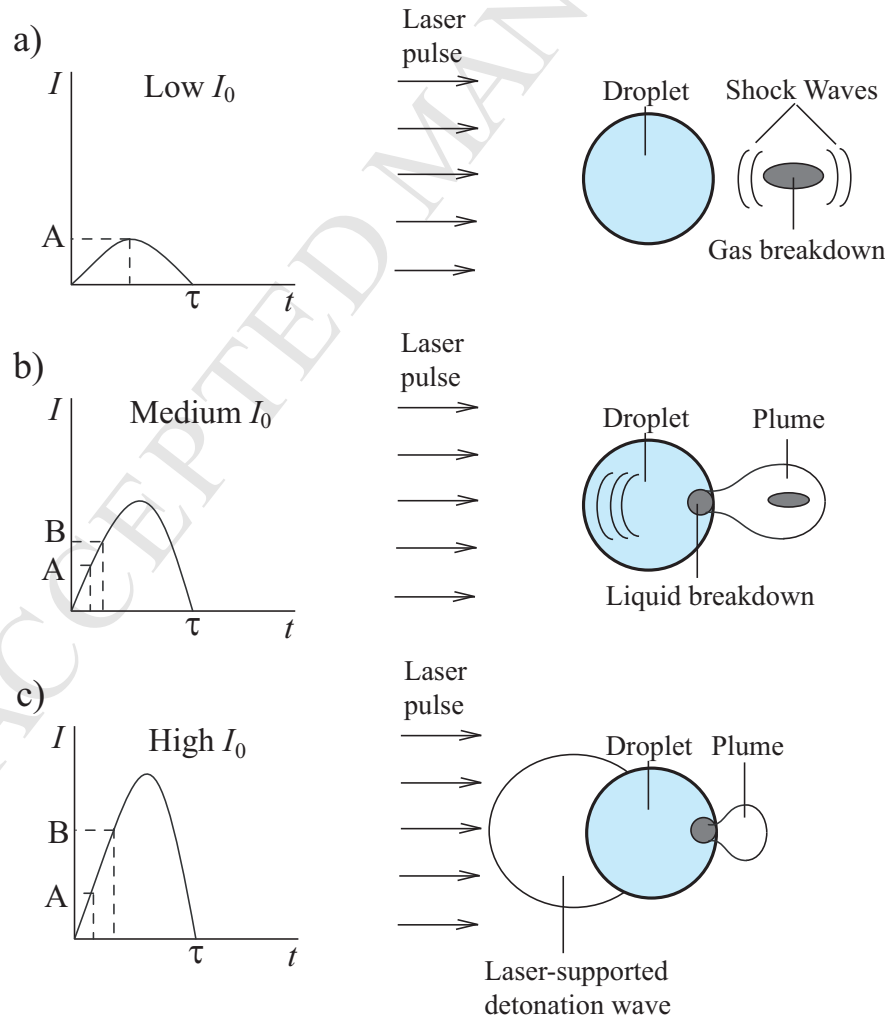

Figure 1. Optical breakdown on a liquid droplet with different intensities of a laser pulse

With a low I_0 (when $I_0 = I_A$), LIB is localized in the gas near the shadow face, and the subsequent portion of the laser pulse sustains the growth of the breakdown (Figure 1a). After the laser pulse, the plasma emission and shock wave propagates away from and towards the droplet. A micrometer-sized transparent droplet acts as a thick lens to focus the input radiation just outside the droplet shadow face and to concentrate the input radiation mainly in a region just inside it. Although the external intensity maximum is an order of magnitude larger than the internal intensity maximum, LIB is initiated within the shadow face of a droplet [15].

With a medium I_0 (when $I_0 > I_B$), LIB in the liquid is initiated when $I_0 = I_B$, although LIB in the gas occurs when $I_0 = I_A$ (Figure 1b). Once LIB has occurred in the liquid, this internal plasma blocks the laser beam from reaching the region outside the shadow face. The plasma in the gas absorbs considerably less energy than the plasma in the liquid. This subsequent portion of the laser pulse therefore sustains the shock wave in the droplet, which ejects the plasma into the gas outside the shadow face and pushes the plasma in the liquid towards the illuminated face.

With a high I_0 (when $I_0 \gg I_B$), the subsequent portion of the laser pulse sustains the shock wave propagating in the liquid towards the illuminated face and then in the gas towards the laser to form a laser-supported detonation wave (Figure 1c). The resultant internal plasma blocks the laser from reaching the region outside the shadow face, and absorbs more of the laser pulse to produce a shock wave and a laser-supported detonation wave.

Processes leading to explosion and optical breakdown of individual droplet have been identified on the basis of existing experimental and computational data (Figure 2). Compared to a metal particle [14], heating and evaporation of a liquid droplet are delayed due to weak absorption of the laser radiation. Concentration of free electrons in the vapor aureole is insufficient for development of an electron avalanche. The key mechanism of development of optical breakdown is explosive evaporation of the droplet.

The laser radiation focuses inside a droplet near its shadow side (Figure 2a). In this region, overheating conditions arise, and the liquid is in a meta-stable state in which its temperature exceeds the temperature of the saturated vapor at a given temperature. An internal vapor cavity is formed, and the liquid boils off in this cavity (Figure 2b). Increase in pressure in the vapor cavity creates conditions for internal micro-breakdown. An internal micro-plasma spot appears and absorbs the laser radiation (Figure 2c). Further increase in pressure in the vapor cavity forms a shock wave expanding inside the droplet (Figure 2d). Expansion of this shock wave induces thermal ionization of the surrounding gas on the shock wave front (Figure 2e). Free electrons that have appeared on the shock wave front induce chain mechanism of breakdown, receiving their energy due to the reverse drag effect (Figure 2f). Intense vaporization of the droplet leads to the thermal destruction of the droplet either by means of local jetting of a part of the droplet mass or by its explosion.

3 Laser pulse

The time of laser pulse, its shape and intensity define the interaction of laser pulse with individual droplet. The intensity of laser pulse is represented as a product of the maximal intensity, I_0, the function describing the time distribution of the intensity, $f_1(t)$, the function taking into account the spatial distribution of the intensity, $f_2(r)$, and the function describing absorption of laser radiation in the medium, $f_3(z)$. The intensity of laser pulse is

$$I(t, r, z) = I_0 f_1(t) f_2(r) f_3(z),$$

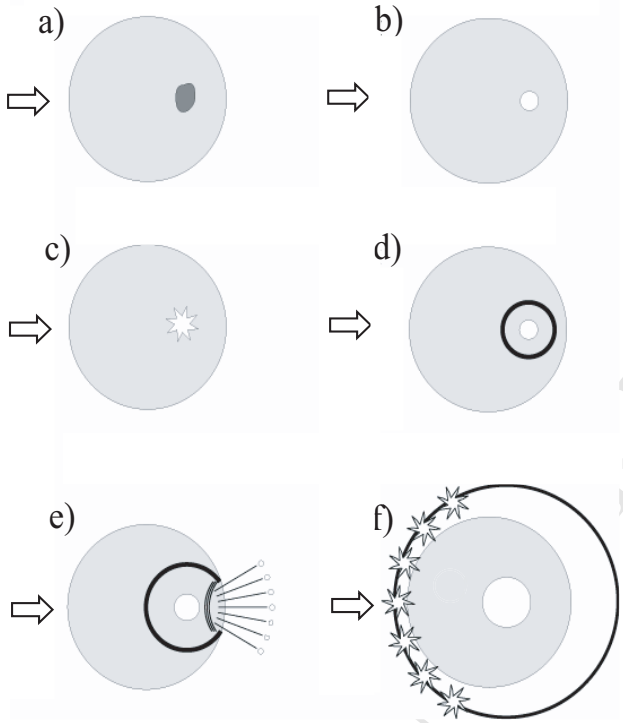

Figure 2. Mechanism of optical breakdown on a liquid droplet

where t is the time, r is the radial coordinate, and z is the coordinate indicating direction of propagation of laser beam.

The theoretical peak intensity of laser pulse at any radial point is calculated for given power and radius of laser spot. The laser does not reach its peak operating power at the moment when it is turned on. It requires a short time to ramp up to its peak output. For a laser pulse which lasts 8 μs, the laser output reaches its peak intensity in about one fourth of a pulse duration and has dropped to roughly three fourth of its peak value when the laser is shut off. The laser model includes a ramp time parameter during which time the laser's output increases linearly to a maximum (Figure 3).

The time distribution of the intensity is represented by a continuous piecewise-linear function

$$f_1(t) = \sum_{k=1}^{N-1} \left[I_k + (I_{k+1} - I_k) \frac{t - t_k}{t_{k+1} - t_k} \right] \phi(t_k, t_{k+1}),$$

where t_k and I_k are the time and the intensity of laser pulse in the ramp point k, and N is a number of ramp points. The function $\phi(t_k, t_{k+1})$ is given by the expression

$$\phi(t_k, t_{k+1}) = \frac{t - t_k + |t - t_k|}{2|t - t_k| + \varepsilon} - \frac{t - t_{k+1} + |t - t_{k+1}|}{2|t - t_k| + \varepsilon},$$

where ε is the small value used to avoid division by zero.

A piecewise-linear representation of the shape of laser pulse is used to compute the integral time parameter of laser pulse

$$S = \int_0^\infty f_1(t)dt = \frac{1}{2} \sum_{k=1}^{N-1} \frac{I_{k+1} + I_k}{t_{k+1} - t_k}.$$

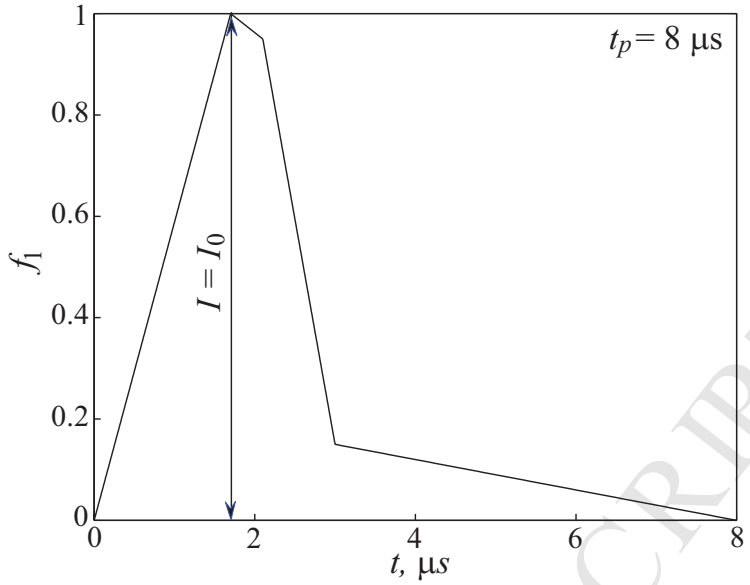

Figure 3. Intensity of laser pulse as a function of time

In a plane normal to the propagation direction of laser pulse, the spatial distribution of the intensity is described by the normal (Gaussian) distribution (Figure 4, where the radius of laser spot is 5 mm)

$$f_2(r) = \exp\left(-\frac{2r^2}{R^2}\right),$$

where r is the radial distance from centreline of the laser beam and R is the radius of laser spot.

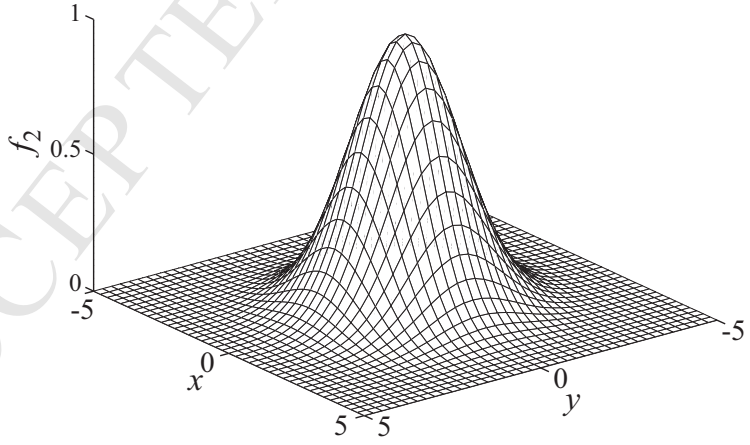

Figure 4. Intensity of laser pulse as a function of radial coordinate

The absorption of laser radiation is described by Bouguer–Lambert–Beer law

$$f_3(z) = \exp\left(-\mu z\right),$$

where μ is the absorption coefficient. The absorption coefficient depends on the nature, aggregate state and volume fraction of particles as well as on the wavelength of laser radiation.

The total energy of laser pulse is related to its intensity

$$Q = \int_0^{\infty} \int_0^{2\pi} \int_0^{\infty} I_0 f_1(t) f_2(r) r dr \, d\varphi \, dt,$$

where φ is the polar angle. Integration over time gives the maximum intensity of laser pulse

$$I_0 = \frac{2Q}{\pi R^2 S}.$$

The total energy of laser pulse is used as the input parameter of the computational model.

4 Mathematical model

Optical breakdown is a complex process involving coupling between droplet and electromagnetic wave interaction, chemical reactions and fluid dynamic effects. However, the estimations show a wide separation in timescales of the laser pulse duration and blast wave propagation. The laser is pulsed on a time scale of some microseconds while the blast wave is observed on a time scale of 10 to 100 μs. Since the plasma forms on the time scale of the laser pulse duration, there is one to two order of magnitude separation in time scales.

4.1 Time scales

Water is material which is commonly used for droplets' generation since its optical, physicochemical and fluidic properties are relatively well known.

To derive mathematical model and justify assumptions, it is necessary to carry out an estimation of time scales of the problem. These are the following

$$\tau_1 = \frac{\rho_s r_s^2}{YD}, \quad \tau_2 = \frac{r_s^2}{a_s}, \quad \tau_3 = \frac{r_s^2}{a_g}, \quad \tau_4 = \frac{r_s^2}{D}, \quad \tau_5 = \frac{c_s \rho_s r_s^2}{\chi_g(T)}, \quad \tau_6 = \frac{r_s}{u_s},$$

where τ_1 is the time of burn-out of a droplet, τ_2 and τ_3 are the transient period of temperature inside and outside a droplet, τ_4 is the transient period of concentration field of the oxidant and combustion products, τ_5 is the time of heating of a droplet up to temperature T with the laser radiation, τ_6 is the time of the gas dynamics processes on the scale equal to the droplet size.

The time scale estimations for a water droplet in air are shown in the Figure 5 using logarithmic scales, where thermal conductivity of the gas is 0.026 W/(m·K), thermal diffusivity of the gas is 2.1×10^{-5} m^2/s, density of the droplet is 1000 kg/m^3, thermal diffusivity of the droplet is 2.3×10^{-5} m^2/s, specific heat capacity of the droplet is 4.2 kJ/(kg·K), oxidant mass fraction is 0.3 kg/m^3, diffusion coefficient of oxidant is 1.8×10^{-5} m^2/s.

The diffusive processes define the evolution of the system on time scales which are much longer than the time of the laser pulse. In calculations, the time of laser pulse is 2.6 μs, and the diffusion is not taken into account. For water droplets $\tau_1 \sim \tau_5$, and the model of thermally thick droplet is used to simulate heating and evaporation of a droplet.

In the explosive vaporization regime, molecular transport effects such as mass diffusion and heat conduction are small compared to convective transport. Convective transport is driven by gradients in the pressure field. Convection becomes important when the vapor pressure of the evaporating droplet becomes comparable to the pressure of the surrounding gas. Under these conditions, the rate of evaporation becomes greater than the rate at which

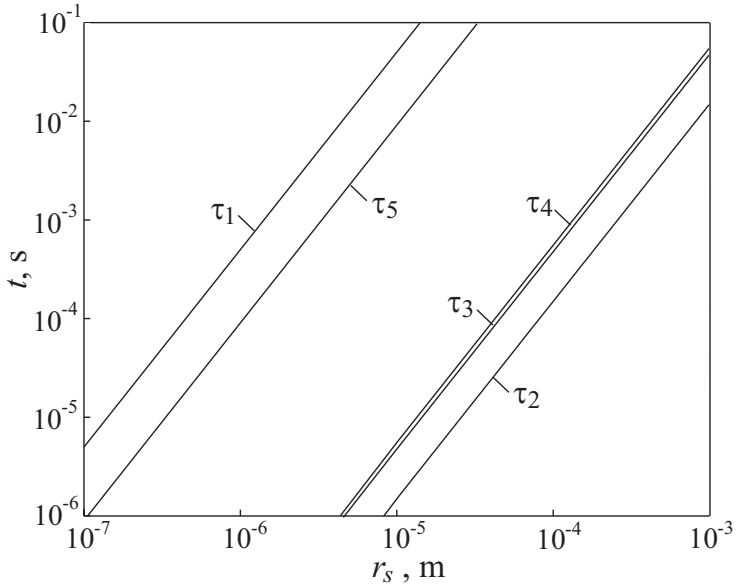

Figure 5. Typical time scales

diffusion can conduct mass away from the droplet. As the temperature and, therefore, the vapor pressure and evaporation rate of the droplet rise, convection becomes an effective mechanism for mass transport away from the droplet.

4.2 Heating and evaporation

In order to describe the heating of a single droplet, when regions of internal focusing with an increased energy release are present because of the effects characterized by the Mie theory, the unsteady heat diffusive equation is solved [13]. In a conservative form, the heat diffusive equation for gas ($k = 1$) and droplet ($k = 2$) with internal heat sources in spherical coordinates is written as

$$\rho_k c_k \frac{\partial T_k}{\partial t} = \frac{1}{r^2}\frac{\partial}{\partial r}\left(r^2 \chi_k \frac{\partial T_k}{\partial r}\right) + G_k(r,t). \tag{1}$$

Here, c is the specific heat capacity, and χ is the thermal conductivity. The source terms, G_1 and G_2, are associated with the chemical reactions in the mixture and with the bulk heat release due to the absorption of laser radiation by a droplet. The source term G_1 is calculated proceeding from the kinetics of combustion of a mixture. The heat input intensity per unit volume of droplet is found from the relation

$$G_2 = \frac{I K_s S_s}{V_s},$$

where S_s is the effective cross-sectional area of droplet, and V_s is the droplet volume. The effectiveness factor of absorption, K_s, is estimated in terms of complex refractive index.

The energy balance equation on the interface between the droplet and surrounding gas (without phase transition on the droplet surface) is written in the form

$$\chi \left.\frac{\partial T}{\partial r}\right|_{r=r_w} - \chi_s \left.\frac{\partial T_s}{\partial r}\right|_{r=r_w} = \mu I(t).$$

Continuity of temperature ($T_s = T$ at $r = r_w$) is applied if the droplet temperature is smaller than the boiling temperature. In the presence of evaporation, the boundary condition on

the droplet surface has the form

$$\chi_s \frac{\partial T_s}{\partial r}\bigg|_{r=r_w} = \rho H_v u_v - \mu I,$$

where u_v is the speed of the evaporation front, and H_v is the specific heat of phase transition.

To perform numerical calculations, a frame of reference related to the droplet surface is used to describe evaporation of droplet. The new coordinate is introduced as $\eta = r/r_w(t)$. Lagrangian formulation of the problem allows to simplify specification of the boundary conditions.

4.3 Vapor cavity

A high-power laser pulse that is focused into a droplet produces a vapor cavity. A mathematical model for the spherically symmetric motion of a laser-induced bubble is used which accounts for gas and liquid compressibility, heat and mass transport effects inside bubble and liquid [28].

In the case of volumetric heat input to a droplet, its central regions become superheated and the liquid in these regions is in the meta-stable state. The boiling off of the liquid to the vapor cavity causes a pressure rise, an expansion of the cavity and a vapor explosion of the droplet. Because the motion of liquid within the droplet is taken to be spherically symmetric and potential, the dynamic equation for droplet with an internal vapor cavity is a generalization of the Rayleigh equation for the motion of gas bubble in infinite liquid

$$\left(1 + \frac{r_b}{r_w}\right)\left(r_b \ddot{r}_b + 2\dot{r}_b^2\right) - \frac{1}{2}\left(1 + \frac{r_b^4}{r_w^4}\right)\dot{r}_b^2 = \frac{p_b - p_w}{\rho/r_w},$$

where p_w and p_b are the pressure on the external boundary of the droplet (at $r = r_w$) and the pressure on the surface of the gas bubble (at $r = r_b$). Dot denotes time differentiation.

The instant of generation of the vapor phase is found using the theory of homogeneous nucleation, which enables one to estimate the time of critical nucleation depending on the degree of superheating and to determine the vapor phase nucleation as a result of variation of the parameters of surrounding liquid [12]. The rate of nucleation is defined by the average number of supercritical nuclei per unit time, and depends on the interfacial surface tension and on the depth of meta-stability. The critical radius of the bubble is calculated in terms of the characteristics of superheating and physical characteristics of the liquid. The Clausius–Clapeyron equation is used to calculate the saturated vapor pressure above the surface of the liquid phase.

In the equilibrium mode of evaporation, the heat absorbed by a droplet is spent to support the processes of phase transition whose intensity is defined by the latent heat of vaporization. The energy balance equation has the form

$$-4\pi r_w^2 \, \chi_s \frac{\partial T_s}{\partial r}\bigg|_{r=r_w} = 4\pi r_w^2 \rho_s H_v \frac{dr_w}{dt}.$$

It is assumed that the transition of superheated liquid to the vapor phase begins at superheated temperatures when the amount of heat stored in the superheated liquid is twice the heat of phase transition.

4.4 Ionization of vapor aureole

Evaporation of a droplet leads to the formation of a vapor aureole. Focusing a laser pulse on a sufficiently small spot size creates high intensities and high electro-magnetic field in the

focal region, resulting in well localized plasma. Further energy is then accumulated by the plasma through absorption, leading to rise of local temperature [9]. The process of electron cascade growth is the dominant effect for breakdown generation. A free seed electron gains kinetic energy by absorbing the energy from the electro-magnetic field of the laser radiation. During collisions with other atoms, new electrons are generated, and the avalanche effect takes place. The mechanism of generation of laser plasma in vapor aureole around the droplet is related to reverse drag effect [14].

Taking the spatial distribution of the laser intensity as a Gaussian shape, calculations are preformed to obtain the distribution of the electron density in the cylindrical focal volume.

The equations describing electron avalanche in the vapor aureole include the equation of heating of vapor aureole due to electron–atom collisions, the equation of warming-up of electrons, the kinetic equation of ionization of vapor as a result of electron impact and the equation of particle mass. These equations are written in the form

$$\begin{aligned}
&\frac{dT_a}{dt} = \frac{6m_e}{5m_a}(T_e - T_a)\alpha\nu;\\
&\frac{dT_e}{dt} = -\left(T_e + \frac{2E}{5k}\right)\frac{1}{\alpha}\frac{d\alpha}{dt} - \frac{6m_e}{5m_a}(T_e - T_a)\nu + \frac{2}{5k}\frac{\mu I}{\alpha n};\\
&\frac{d\alpha}{dt} = \frac{C}{T_e^{9/2}} n\left[\alpha(1-\alpha)\frac{\beta^2 n}{1-\beta} - \alpha^3 n\right];\\
&\frac{dm_s}{dt} = -\frac{K_s I A_s}{V_v}.
\end{aligned}$$

Here, m is the mass, n is the number density of heavy particles, α is the degree of ionization, ν is the collision frequency of electrons with atoms and ions, E is the potential of ionization, A_s is the surface area of droplet, K_s is the factor describing efficiency of absorption of laser radiation by droplet, V_v is the volume of vapor aureole, and $C = 1.05 \times 10^{-8}$ cm^6·K$^{9/2}$. The equilibrium degree of ionization, β, is defined from Saha equation for the temperature of evaporation. Subscripts e and a correspond to the electrons and atoms, subscript v corresponds to the vapor and subscript p corresponds to the droplet.

The induction period of chemical reaction is separated in time with the laser pulse, and no significant energy contribution is expected from the chemical reactions. This enables one to find the parameters of the mixture from the simplified model, assuming that the mixture is adiabatically compressed by the vapor cavity.

4.5 Propagation of shock wave

To describe gas dynamic processes inside and outside a single droplet, the model consisting of conservative equations of mass, momentum, energy and species for a mixture of ideal multi-component non-viscous and non-conducting components (Euler equations) is used. In the explosive vaporization regime, molecular transport effects such as diffusion and conduction are small compared to convective transport [31]. The plasma in vapor aureole is considered as an ideal gas. The Euler equations are used to describe the plasma expansion in vapor aureole (for simplicity, this process is assumed to be spherically symmetric). These equations are written in the form

$$\frac{\partial U}{\partial t} + \frac{\partial F}{\partial r} = H.$$

The flow variables vector, the flux vector and the source term are

$$U = \begin{pmatrix} \rho \\ \rho u \\ \rho e \\ \rho Y_i \end{pmatrix}, \quad F = \begin{pmatrix} \rho u \\ \rho u^2 + p \\ (\rho e + p)u \\ \rho Y_i u \end{pmatrix}, \quad H = \begin{pmatrix} 0 \\ 0 \\ 0 \\ \omega_i \end{pmatrix}.$$

Here, t is time, ρ is the density, u is the velocity, p is the pressure, e is the specific total energy, Y_i is the mass fraction of the ith component of the mixture, ω_i is the rate of formation/consumption of ith component. The equation of state of an ideal gas is

$$p = \rho RT \sum_{i=1}^{N_c} \frac{Y_i}{\mu_i},$$

where μ_i is the molecular weight of the ith component and R is the universal gas constant. The specific internal energy and equation of state are used to find the thermodynamic properties of the mixture, its temperature and pressure. The temperature dependence of the specific heat capacities of the components are presented in the form of a fourth-order polynomial (JANAF tables).

The actual reaction is a multiple-step reversible reaction which is composed of many elementary steps. A large amount of effort has been devoted to the development of detailed and reduced kinetic mechanisms. The overall reaction order and overall activation energy are important to characterize overall gas dynamics pattern and temperature of the mixture. The chemical reaction is assumed to be an irreversible single step reaction. The heat effect of the reaction calculated from the enthalpies of formation of the reactants and products of reaction.

4.6 Optical properties

A set of Mie functions is used to compute the four Mie coefficients, efficiencies of extinction, scattering, backscattering and absorption, and the two angular scattering functions [21]. The input parameters are the complex refractive index of the sphere relative to the ambient medium and the size parameter [20]. The complex refractive index is $n = n_1 + in_2$, where the real part n_1 is the refractive index and indicates the phase velocity, while the imaginary part n_2 is the extinction coefficient indicating the amount of attenuation loss when the electromagnetic wave propagates through the material. The size parameter is $x = kr_s$, where r_s is the sphere radius and k the wave number in the ambient medium ($k = 2\pi/\lambda$).

The efficiencies Q_i for the interaction of radiation with a scattering sphere of radius r_s are cross sections σ_i normalized to the particle cross section, πr_s^2, where subscript i stands for extinction ($i = ext$), absorption ($i = abs$), scattering ($i = sca$), backscattering ($i = bsc$), thus $Q_i = \sigma_i^2/\pi r_s^2$. Energy conservation requires that $\sigma_{ext} = \sigma_{sca} + \sigma_{abs}$. The scattering efficiency, Q_{sca}, follows from the integration of the scattered power over all directions, and the extinction efficiency, Q_{ext}, follows from the extinction theorem (forward-scattering theorem).

5 Computational procedure

Equations describing heating and explosive evaporation of droplet and development of electron avalanche are solved numerically to obtain the threshold irradiance required to produce breakdown for a given pulse duration, using a Runge–Kutta fourth order technique with

adaptive time step. Optical breakdown is assumed to occur when the free electron density obtained during the laser pulse exceeds the given critical value (10^{19}–10^{20} cm^{-3}).

Gas dynamics equations describing propagation of shock wave inside droplet and surrounding gas are solved with finite volume method. Non-linear CFD solver works in an explicit time marching fashion, based on a three-step Runge–Kutta stepping procedure and piecewise parabolic method. The governing equations are solved with Chakravarthy–Osher scheme for inviscid fluxes. Details on the implementation of the computational procedure for the two-phase flow model are provided in [33].

6 Results and discussion

The estimation of the threshold conditions of breakdown involves the successive solution of problems such as the heating of a droplet to the temperature of explosive transformation, the generation of shock wave of explosion products, the recording of the initial concentration of free electrons in gas due to thermal ionization behind the shock wave front, and the development of an electron avalanche in the vapor cavity. The source of laser radiation is provided by a pulsed chemical HF laser with the following characteristics: time os laser pulse is $t_p = 2.6$ μs, wavelength is $\lambda = 4.2$ μm, radius of laser spot is $R = 5$ mm, temporal characteristic os laser pulse is $S = 1.5$ μs. Droplet location relative to the centerline of the laser beam, total energy and shape of laser pulse vary in the calculations. In all simulations, a Gaussian intensity profile in time is assumed.

The high intensity radiation from a laser produces a plasma. Unlike water which is almost transparent to the incident radiation, the plasma absorbs much of the laser energy and converts it to heat. Explosion takes place when the superheating temperature of the liquid nearby the plasma is reached.

Mie efficiencies are plotted versus size parameter in the Figure 6 for liquid sphere ($n = 2 + i0.01$). A large number of spherical harmonics have to be computed. The parameter with the maximum values and with the largest fluctuations is the efficiency of back-scattering (line 4). The lines 1 (efficiency of extinction) and 2 (efficiency of scattering) follow each other closely near the values of 2. The lowest line (line 3) shows efficiency of absorption.

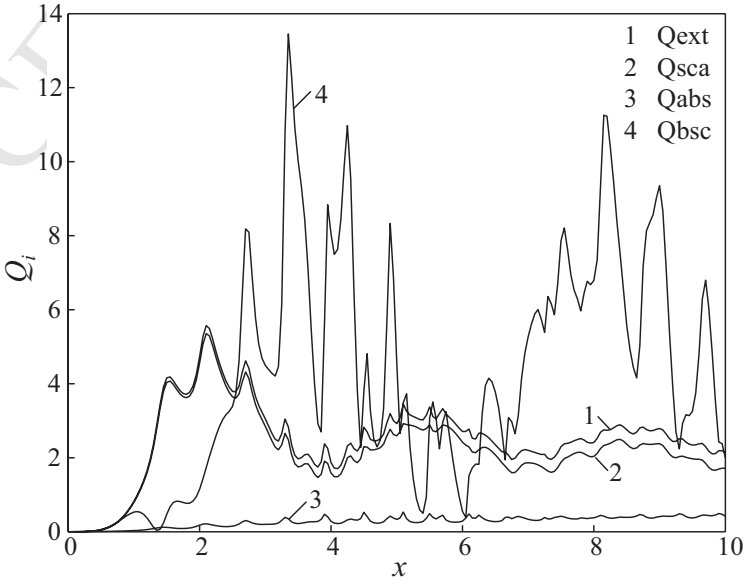

Figure 6. Mie efficiencies for liquid sphere

The complex scattering amplitudes, S_1 and S_2, are displayed on polar diagram in the form of Mie scattering intensities ($|S_1|^2$ in the upper half of circle and $|S_2|^2$ in the lower half of circle) showing the detailed shape of the scattering pattern. Both functions are symmetric with respect to both half circles. The angular dependencies of the scattered power in the two polarizations are plotted in the Figure 7 for liquid sphere. For liquid sphere, scattering in the backward hemisphere is larger than in the forward hemisphere.

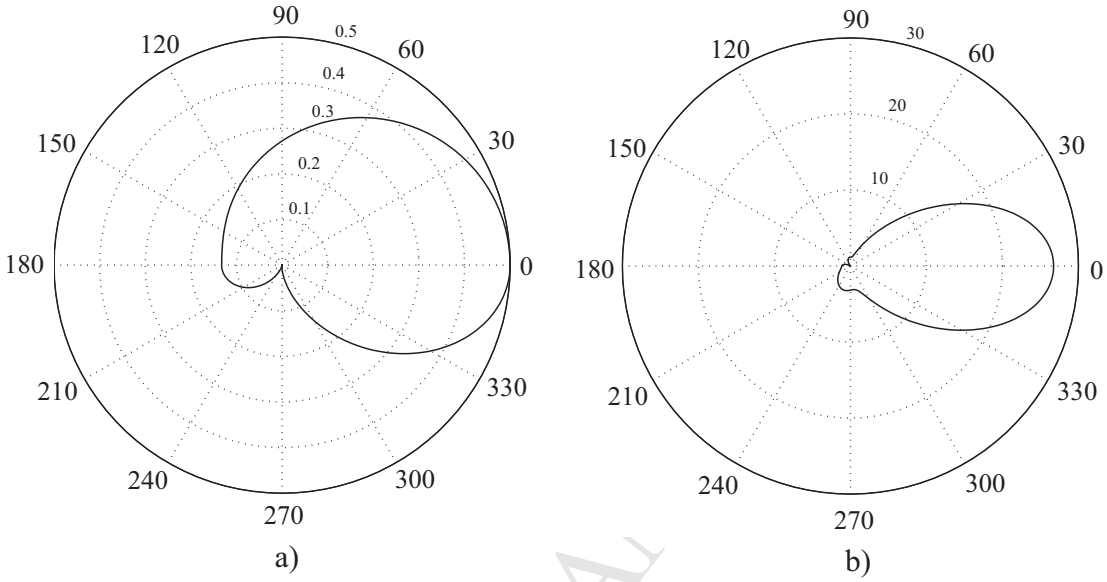

Figure 7. Angular Mie scattering diagrams for liquid sphere at $x = 1$ (a) and $x = 2$ (b)

The temperature field in a water droplet and surrounding gas is shown in the Figure 8. The laser beam falls on the droplet from right to left. A local temperature rise is observed on the exposed surface of the droplet. A thin thermal boundary layer is formed in the vicinity of the droplet. An increase in temperature inside the droplet corresponds to the center of an internal vapor cavity. The droplet is superheated, and water is in the meta-stable state. In this region, ionization process is likely to occur. Line 7 corresponds to the start of the explosive process at a temperature of 698 K. The time of explosive transformation of a droplet is 1.55 μs.

The droplet temperature depends on the energy of laser pulse. The heating of a droplet to the boiling temperature with subsequent evaporation depends significantly on the droplet position. The droplets which are peripheral with respect to the beam centerline do not reach the mode of developed vaporization and fail to develop conditions for the beginning of the plasma generating process. Because the radiation intensity varies as a function of the distance from the beam centerline by the Gaussian law, the breakdown occurs at different times. No conditions of breakdown are observed for the droplet that is the most remote from the centerline.

The plasma formation becomes almost non-transparent to laser radiation, which brings about an increase in the temperature and pressure of the evaporation products, as well as about the emergence of an unsteady flow in the neighborhood of micro-plasma formation. The expansion of plasma formation generates a strong shock wave whose intensity decreases with increasing distance from the droplet center (Figure 9).

Two shock waves are developed. One shock wave exists in the water region and faces toward the origin. The second shock exists in the air and faces away from the origin. The contact discontinuity, which is the remnant of the initial discontinuity, separates the water from the air. The contact discontinuity is characterized by a discontinuous change

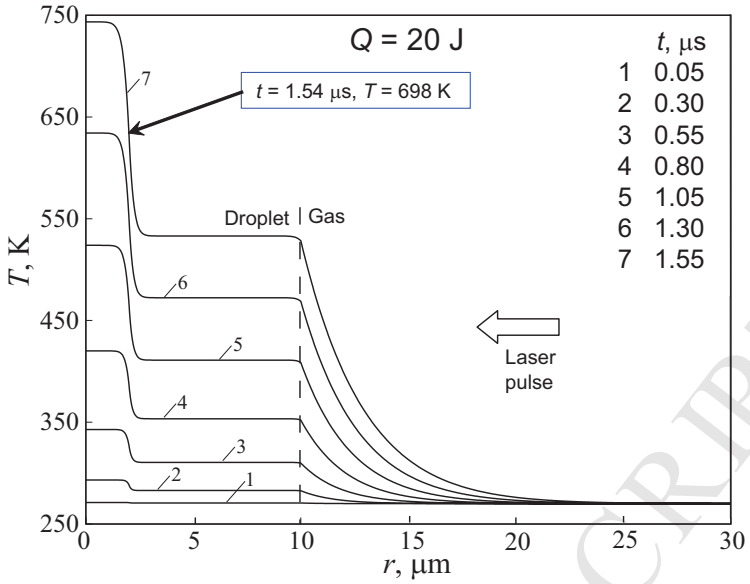

Figure 8. Temperature field inside and outside droplet

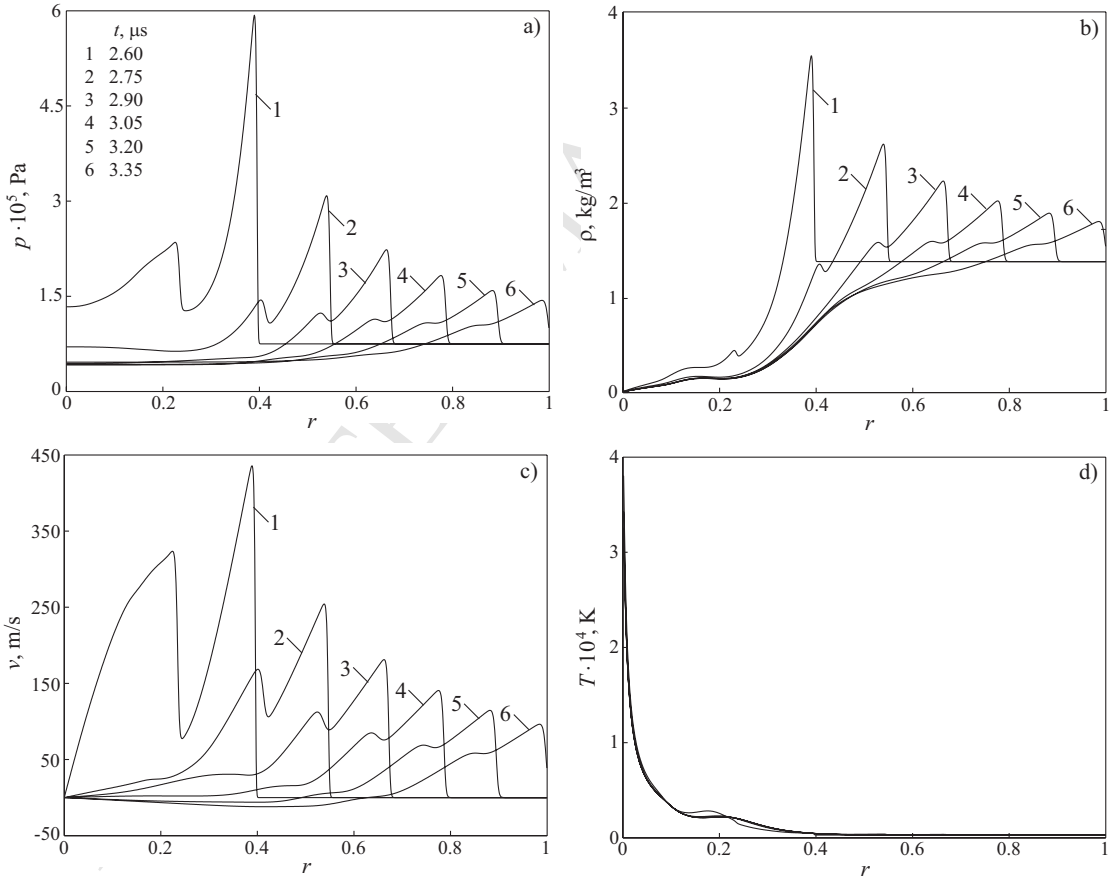

Figure 9. Pressure (a), density (b), velocity(c) and temperature (d) distributions inside droplet

in density and temperature, and continuous pressure and velocity profiles. Shock waves are discontinuous in all of the flow variables. The region between the water shock and the origin is a region of strong expansion.

The shock pressure decreases faster with increasing propagation distance than in the acoustic limit, where a pressure decay proportional $1/r$ would be expected for a spherical

source. The fast pressure decay is caused by the energy dissipation at the shock front and the non-linearity of propagation, which results in a modification of the pressure profile during propagation. The speed of propagation increases with increasing pressure, causes the trailing edge of a shock wave to propagate significantly slower than the leading edge, resulting in shock wave broadening. This shock wave broadening is most pronounced in high pressure regions (near the droplet). Based on the conservation of momentum, a $1/r^2$ dependence of the shock pressure can be derived if shock wave broadening is negligible. This relationship is in reasonable agreement with experimental data obtained with nanosecond and picosecond pulses at distances above 100 μm.

The air is shock-heated to temperatures high enough to cause ionization. If the ionized air is subjected to more radiation, avalanche breakdown of the air occurs. The simulation substantiates the theory that shock heating of air is responsible for droplet enhanced breakdown.

The plasma spot is non-transparent to laser radiation. An increase in pressure and temperature induces the expansion of a shock wave. Its intensity decreases with increase in distance from the center of the vapor cavity. Tables from 1 to 3 show LIB conditions depending on the droplet radius and the total energy of the laser pulse. The first column corresponds to the total energy of laser pulse. The second column indicates the time of explosive transformation. The third column gives the degree of ionization. The fourth column indicates validation of the condition of explosive transformation. The fifth column indicates the presence or absence of an electron avalanche.

Table 1. Breakdown conditions for droplet of 5 μm

Q, J	t_e, μm	α	$T > T_e$	Yes/No
5	—-	—	—	—
10	1.83	10^{-2}	+	+
15	1.38	10^{-2}	+	+
20	1.13	10^{-2}	+	+
30	0.93	10^{-2}	+	+
50	0.72	10^{-2}	+	+

Table 2. Breakdown conditions for droplet of 10 μm

Q, J	t_e, μm	α	$T > T_e$	Yes/No
5	—-	—	—	—
10	—-	—	—	—
15	1.41	10^{-5}	+	+
20	1.16	10^{-2}	+	+
30	0.96	10^{-2}	+	+
50	0.77	10^{-2}	+	+

Table 1 shows that, in the case of a droplet with radius of 5 μm, a breakdown is realized at an energy of $Q = 10$ J. An increase in the droplet size causes an increase in the time required for its heating and a decrease in the degree of ionization behind the shock wave. However, the Table 2 shows that the energy of $Q = 15$ J is estimated to be sufficient for initiating a laser breakdown. At droplet radius of 20 μm, the initial degree of ionization behind the shock wave decreases. As a result, no electron avalanche develops for low energies of laser pulse, and the threshold of plasma generation increases to $Q = 30$ J as presented in the Table 3.

Table 3. Breakdown conditions for droplet of 20 μm

Q, J	t_e, μm	α	$T > T_e$	Yes/No
5	—-	—	—	—
10	—-	—	—	—
15	1.48	10^{-11}	+	—
20	1.23	10^{-11}	+	—
30	1.04	10^{-11}	+	+
50	0.83	10^{-11}	+	+

The heating occurs earlier in the pulse at higher intensity, giving rise to earlier expansion of the plasma and decrease of its density. However, the temperature increases with intensity, because even if the absorption drops with the density, the energy deposited in the target increases.

The optical breakdown is a result of the competition between three factors: (i) heating a droplet to the temperature of explosive transformation (at low laser pulse energy, the large droplets do not have enough time for being heated, and the small droplets exchange heat intensively with the surrounding), (ii) intensity of the shock wave contributing to the thermal ionization of vapor (for large droplets, the intensity of shock wave is low), (iii) development of an electron avalanche.

The radius of laser spot has a significant impact on the threshold energy of optical breakdown. For droplet radius of 5 μm, a breakdown takes place at energy of $Q = 10$ J. Increase in droplet radius leads to increase in time of droplet heating and decrease in degree of ionization. No electron avalanche develops at low intensity of laser pulse, and threshold energy of optical breakdown increases.

7 Conclusion

The injection of liquid droplets with low evaporation temperature causes optical breakdown on the individual droplet and leads to a drop of the minimum pulse energy of detonation in the gas-droplet mixture. Processes leading to explosion and optical breakdown of individual droplet have been identified on the basis of existing experimental and computational data, and mathematical models and numerical methodology for computer modelling of various stages of the optical breakdown on individual droplet are developed. Sub-models of optical breakdown on liquid droplet include droplet heating to boiling temperature, its evaporation and formation of vapor aureole around the droplet, ionization of vapor aureole and development of electron avalanche, appearance of micro-plasma spots and their expansion, propagation of shock wave inside droplet and in the surrounding gas.

The threshold intensity of optical breakdown on individual water droplet and its dependence on droplet radius, location of droplet, total energy and radius of laser spot are studied. Occurrence of LIB is a result of the competition between different factors including time of heating a droplet to the temperature of explosive transformation, intensity of the shock wave contributing to the thermal ionization of vapor and time of development of an electron avalanche.

Acknowledgements

This work was financially supported by the Ministry of Education and Science of Russian Federation (agreement No 14.574.21.0151, unique identifier of applied scientific research RFMEFI57417X0151).

References

[1] Phylippov Yu.G., Dushin V.R., Nikitin V.F., Nerchenko V.A., Korolkova N.V., Guendugov V.M. Fluid mechanics of pulse detonation thrusters. Acta Astronautica, 2012, 76(1), 115–126.

[2] Smirnov N.N., Betelin V.B., Nikitin V.F., Phylippov Yu.G., Jaye Koo. Detonation engine fed by acetylene-oxygen mixture. Acta Astronautica, 2014, 104(1), 134–146.

[3] Smirnov N.N., Nikitin V.F., Dushin V.R., Filippov Yu.G., Nerchenko V.A., Khadem J. Combustion onset in non-uniform dispersed mixtures. Acta Astronautica, 2015, 115(1), 94–101.

[4] Smirnov N.N., Betelin V.B., Kushnirenko A.G., Nikitin V.F., Dushin V.R., Nerchenko V.A. Ignition of fuel sprays by shock wave mathematical modeling and numerical simulation. Acta Astronautica, 2013(1), 87, 14–29.

[5] Li X.-Q., Hong Y.-J., He G.-Q., Wen M. The interaction between laser and water droplets. Lasers in Engineering, 2006, 16(1–2), 381–391.

[6] Qin Q., Attenborough K. Characteristics and application of laser-generated acoustic shock waves in air. Applied Acoustics, 2004, 65(4), 325–340.

[7] Demos S..G., Negres R.A., Raman R.N., Shen N., Rubenchik A.M., Matthews M.J. Mechanisms governing the interaction of metallic particles with nanosecond laser pulses, Optics Express, 2016, 24(7), 7792-7815.

[8] Biswas A., Pinnick R.G., Xie J.-G., Ruekgauer T.E., Armstrong R.L. Observations of stimulated Raman scattering and laser-induced breakdown in millimeter-sized droplets. Optics Letters, 1992, 17(22), 1569–1571.

[9] Kopecek H., Maier H., Reider G., Winter F., Winther E. Laser ignition of methane–air mixtures at high pressures. Experimental Thermal and Fluid Science, 2003, 27(4), 499–503.

[10] Fan C.H., Sun J., Longtin J.P. Breakdown threshold and localized electron density in water induced by ultrashort laser pulses. Journal of Applied Physics, 2002, 91(4), 2530–2536.

[11] Műsing A., Riedel U., Warnatz J., Herden W., Ridderbusch H. Laser-induced breakdown in air and behind droplets: a detailed Monte Carlo simulation. Proceedings of the Combustion Institute, 2007, 31(2), 3007–3014.

[12] Emelyanov V.N., Volkov K.N. Calculation of the threshold power of optical breakdown during interaction between a laser pulse and droplets of dielectric liquid. High Temperature, 2005, 43(3), 344–351.

[13] Emelyanov V.N., Volkov K.N. Modelling of the interaction of a pulse of laser radiation with a liquid droplet. Journal of High Temperature and Material Processes, 2006, 10(1), 141–159.

[14] Emelyanov V.N., Volkov K.N. Numerical simulation of laser-induced detonation in mixture of hydrogen with suspended metal particles. International Journal of Hydrogen Energy, 2014, 39(11), 6222–6232.

[15] Chang R.K, Eickmans J.H., Hsieh W.-F., Wood C.F., Zhang J.-Z., Zheng J. Laser-induced breakdown in large transparent water droplets. Applied Optics, 1988, 27(12), 2377–2385.

[16] Eichmans J.H., Hsieh W.F., Chang R.K. Laser-induced explosion of H_2O droplets: spatially resolved spectra. Optical Letters, 1987, 12(1), 22–24.

[17] Kafalas P., Ferdinand A.P. Fog droplet vaporization and fragmentation by a 10.6 μm laser pulse. Journal of Applied Optics, 1973, 12(1), 29–33.

[18] Kafalas P., Herrmann J. Dynamics and energetics of the explosive vaporization of fog droplets by a 10.6 μm laser pulse. Journal of Applied Optics, 1973, 12(4), 772–775.

[19] Hsieh W.-F., Eickmans J.H., Chang R.K. Internal and external laser-induced avalanche breakdown of single droplets in an argon atmosphere. Journal of the Optical Society of America, 1987, 4(11), 1816–1820.

[20] Datsyuk V.V., Izmailov I.A. Optics of microdroplets. Advances in Physical Sciences, 2001, 44(10), 1061–1073.

[21] Wriedt Th. Mie theory: a review / The Mie theory: basics and applications. Springer, 2012, 53–71.

[22] Pinnick R.G., Biswas A., Armstrong R.L., Jennings S.G., Pendleton J.D., Fernandez G. Micron-sized droplets irradiated with a pulsed CO2 laser: measurement of explosion and breakdown thresholds. Applied Optics, 1990, 29(7), 918–925.

[23] Favre C., Boutou V., Hill S.C., Zimmer W., Krenz M., Lambrecht H., Yu J., Chang R.K., Woeste L., Wolf J.-P. White-light nanosource with directional emission. Physical Review Letters, 2002, 89(3), 035002.

[24] Thoroddsen S.T., Takehara K., Etoh T.G., Ohl C.-D. Spray and microjets produced by focusing a laser pulse into a hemispherical drop. Physics of Fluids, 2009, 21(11), 112101.

[25] Tagawa Y., Oudalov N., Visser C.W., Peters I.R., van der Meer D., Sun C., Prosperetti A., Lohse D. Highly focused supersonic microjets. Physical Review, 2012, 2(3), 031002.

[26] Zemlyanov A.A., Kuzikovskii A.V., Chistyakova L.K. On the mechanism of optical breakdown under interaction of water targets by the radiation from a pulsed of CO_2 laser. Technical Physics, 1984, 51(7), 1439–1444.

[27] Loskutov V.S., Strelkov G.M. On explosive evaporation of a water droplet under the action of laser pulses at 1.06 and 2.36 μm. Optical Spectroscopy, 1982, 53(5), 888–892.

[28] Emelyanov V.N., Li Solong, Volkov K.N. Heat and mass transfer in gas-dispersed systems exposed to intense radiation. Heat Transfer Research, 2003, 34(5–6), 38–50.

[29] Mamonov V.K. Experimental study of the apperance and development of an optical discharge wave at a breakdown in water droplets. Technical Physics, 1986, 56(12), 2410–2412.

[30] Auguste T., Gaufridy de Dortan F., Ceccotti T., Hergott J. F., Sublemontier O., Descamps D., Schmidt M. Numerical study of nanosecond laser interactions with micro-sized single droplets and sprays of xenon. Journal of Applied Physics, 2007, 101(4), 043302.

[31] Carls J.C., Brock J.R. Explosion of a water droplet by pulsed laser heating. Aerosol Science and Technology, 1987, 7(1), 79–90.

[32] Volkov K.N. Combustion of single aluminium droplet in two-phase flow / Heterogeneous Combustion. Nova Science, 2010, 191–260.

[33] Volkov K. Numerical analysis of Navier–Stokes equations on unstructured meshes / Handbook on Navier–Stokes equations: theory and analysis. Nova Science, 2016, 365–442.

Numerical Simulation of Optical Breakdown in a Liquid Droplet Induced by a Laser Pulse

P.V. Bulat[1, 2], O.P. Minin[3], K.N. Volkov[4]

[1]ITMO University, St Petersburg, Russia
[2]Baltic State Technical University, St Petersburg, Russia
[3]Public Joint-Stock Company "Tupolev", Moscow, Russia
[4]Kingston University, London, United Kingdom

- Processes leading to optical breakdown of individual droplet are identified
- Mathematical models of various stages of optical breakdown are developed
- Threshold intensity of optical breakdown is calculated
- Occurrence of optical breakdown on individual droplet is studied